Smart Structures and Systems, *Vol. 27, No. 6 (2021) 969-982*
DOI: https://doi.org/10.12989/sss.2021.27.6.969

Double-frequency passive deformation sensor based on two-layer patch antenna

Songtao Xue [1,2a], Zhuoran Yi [1b], Liyu Xie*[1] and Guochun Wan [3]

[1] *Department of Disaster Mitigation for Structures, Tongji University, Shanghai, China*
[2] *Department of Architecture, Tohoku Institute of Technology, Sendai, Japan*
[3] *Department of Electronic Science and Technology, Tongji University, Shanghai, China*

(*Received May 17, 2020, Revised October 30, 2020, Accepted February 20, 2021*)

Abstract. To avoid the issues of incomplete strain transfer ratio and insufficient bonding strength of a monolithic stressed antenna, this paper presents an unstressed deformation sensor based on two-layer patch antenna for structural health monitoring. The proposed sensor is composed of a monolithic patch antenna and a stacked patch generating two fundamental resonant frequencies within a 3-to-7 GHz band. The resonant frequencies' shifts caused by the offset of the stacked patch were selected as the sensing parameters. An equivalent circuit was used to analyze the sensing method, which shows the relative displacement to be linear to the shift of resonant frequencies. This phenomenon was then checked by numerical simulation using the Ansoft High Frequency Structure Simulator 15 (HFSS15) and experiments in laboratory using both wired and wireless setups. Furthermore, the accuracy of measurement is verified to be increased by combining two resonant frequencies.

Keywords: passive wireless sensor; two-layer patch antenna; deformation monitoring; coupling stacked patch; resonant frequency

1. Introduction

Nowadays, structure health monitoring for structural deficiencies is of great importance to the prevention of casualties caused by unforeseen structure collapse (Soman *et al*. 2014, Abdulkarem *et al*. 2019), and superfluous deformation induced by earthquakes, typhoons, floods or aging is one of the most influential deficiencies (Leung *et al*. 2000, Woo *et al*. 2011). The detection of deformations such as displacement, cracks, and deflections have become a part of cutting-edge research in recent years (Moreno-Gomez *et al*. 2018).

To circumvent the inconvenience brought by deployed power and data cables as well as the batteries of wired sensors, the passive wireless deformation sensor is very promising (McGee *et al*. 2019). Use of the monolithic patch antenna as a deformation sensor has been fully investigated due to its low-cost, low-profile, conformable properties, and easy fabrication (Ayyildiz *et al*. 2019). A typical patch antenna sensor monitors structural deformation by attaching a monolithic patch antenna onto the surface of a structure (Cho *et al*. 2016, Mohammad *et al*. 2011, Mohammad and Huang 2010, Yi *et al*. 2013). Strains, displacements, or cracks induced by the structural members would cause deformation of the antenna, leading to a resonant frequency shift of the patch. This monolithic antenna sensor simultaneously has temperature compensation (Tchafa and Huang 2018, Sanders *et al*. 2015, Yao *et al*. 2016) and other advantages such as easy fabrication (Yi *et al*. 2016). However, the antenna needs to be stressed during the service time. Meanwhile, the issues of incomplete strain transfer ratio, insufficient bonding strength, and randomness of crack propagation remain unsolved (Xue *et al*. 2019b). These problems will hinder the antenna sensor's practical use due to the problems with on-site calibration of sensors and durability issues of adhesive materials.

To avoid the above-mentioned issues, several deformation sensors with unstressed sensing units are proposed (Bhattacharyya *et al*. 2009, Xue *et al*. 2019a, b, c, Xue *et al*. 2020a, b). As for patch antenna sensors, the relative position between a monolithic patch antenna and an interacting component was designated to be a sensing unit for displacement, instead of using the elongated or compressed deformation of a whole patch. Bhattacharyya *et al*. (2009) proposed an unstressed displacement sensor by measuring the resonant frequency shift caused by the relative displacement between the RFID tag and patch antenna. Xue *et al*. (2019b) presented a crack sensor based on a patch antenna, which is fed by a pair of microstrip lines forming a parallel plate capacitor. The crack width can be sensed by measuring the relative movement between two microstrip lines without any stress in the patch antenna. Xue *et al*. (2019a) also designed a crack sensor formed by a monolithic patch antenna and an overlapped sub-patch. The copper radiation side of the overlapped sub-patch is stacked on the metal radiation patch of the underlying monolithic patch and shortened by it; then, the combination forms a

*Corresponding author, Associate Professor,
E-mail: liyuxie@tongji.edu.cn
[a] Professor, E-mail: xue@tongji.edu.cn
[b] M.D. Student, E-mail: yzr1997@tongji.edu.cn

ISSN: 1738-1584 (Print), 1738-1991 (Online)

length-adjustable radiation patch. The electric length of the combined patch antenna can change with the movement of the sub-patch, leading to a shift of resonant frequency in the sensing system. This detachable structure prevents the antenna from being stretched, and it also improves its usability without on-site calibration. Inevitably, the precision of these unstressed sensors is still affected by environmental disturbance. However, by evaluating several resonant frequencies or other parameters simultaneously, the accuracy of measurement can be improved (Tchafa and Huang 2018, Mohammad and Huang 2012, Marindra and Tian 2019).

The multilayer patch antenna is another feasible solution as an unstressed deformation sensing unit. A typical multilayer patch antenna consists of a bottom monolithic patch antenna and several parallel copper patches (Yadava and Vishvakarma 2000). Different from the previous crack sensor with an overlapped sub-patch (Xue *et al*. 2019a), an open-circuit is formed between the parallel radiation patch and bottom radiation patch; then, the two adjacent copper patches are separated by a middle dielectric board. While the previous design using the overlapped sub-patch to extend the length of the radiation patch and further change the resonant frequency, this design mainly focuses on strengthen or weaken the coupling factor between two adjacent radiation patches. In general, the multilayer patch antenna owns multiple coupling resonant frequencies due to the vertical formation of the resonant elements (Pandey and Vishvakarma 2005, Chung and Mohan 2003, You *et al*. 2007). This technology has been used recently to adjust bandwidth (Malekpoor and Hamidkhani 2019). Rajo-Iglesias *et al*. (2001, 2002, 2004) investigated the relationship between the resonant frequencies and the relative displacement of stacked patches. Because the stacked patch moved from the center to the edge of the monolithic patch antenna, the two resonant frequencies tended to move away from each other. This phenomenon was mainly caused by the decrease of coupling factor, which would redistribute the surface current and then alter the electric length (Waterhouse 2007). The dislocation of the dielectric load would shift the effective length of the resonant patch and further change the resonant frequencies. If the shift of resonant frequencies is linear enough with the relative movement of stacked patches, the multilayer patch antenna could be selected as an unstressed patch antenna sensor by sensing the offset of the parallel copper patches. Furthermore, the accuracy could be sufficiently improved by simultaneously measuring multiple coupling resonant frequencies.

In order to improve the accuracy by multiparameter sensing, this paper proposed a double-frequency deformation sensor based on a two-layer patch antenna. This sensor consists of a monolithic patch antenna and a parallel radiation patch, as well as two fundamental resonant frequencies caused by the resonance in two radiation patches and shifted by the change of coupling between each other. These two resonant frequencies were taken into consideration in the measurement to improve the measuring accuracy. Since the coupling mainly depends on the location of the parallel radiation patch, the relative displacement between the parallel patch and the monolithic patch antenna could be determined by measuring the resonant frequencies shift (Waterhouse 2007).

This paper is organized as follows. Section 2 introduces the concept of a deformation sensor based on the two-layer patch antenna and illustrates the sensing mechanism. This section introduces the innovative concept of two prototypes of the deformation sensor for wired and wireless measurement. In Section 3, the appropriate dimension parameters are determined for the sensing system. Section 4 describes the fabrication of sensors and the instrumentation setup of experiments. Both wired and wireless interrogations are analyzed in this section. Conclusions are then drawn, and future research potential is discussed.

2. Crack sensor based on two-layer microstrip patch antenna

In the configuration of the multilayer microstrip patch antenna, two or more patches on different layers of the dielectric substrate are stacked on each other (Waterhouse 2007), which is shown in Fig. 1(a). A multilayer microstrip patch antenna has multiple fundamental resonant frequencies for each parallel radiation patch. These fundamental resonant frequencies would be coupled with each other as the distance between the radiation patches is much lower than a quarter wavelength of the antenna, and the dislocation of each radiation patch would cause the shift of the multiple resonant frequencies (Pandey and Vishvakarma 2005, You *et al*. 2007). In fact, the coupling factor between the stacked patches and monolithic patch

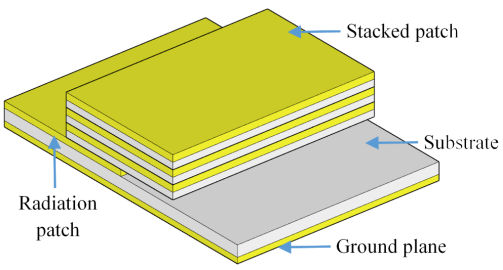

(a) Axonometric drawing of multilayer patch antenna

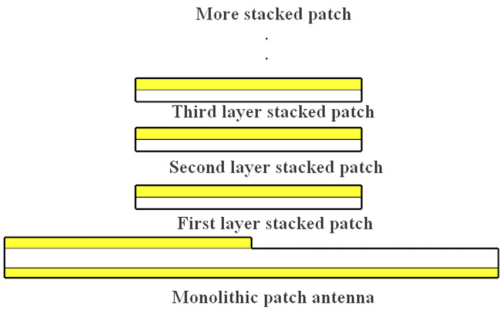

(b) Front view of multilayer patch antenna

Fig. 1 Concept figures of multilayer patch antenna and two-layer patch antenna

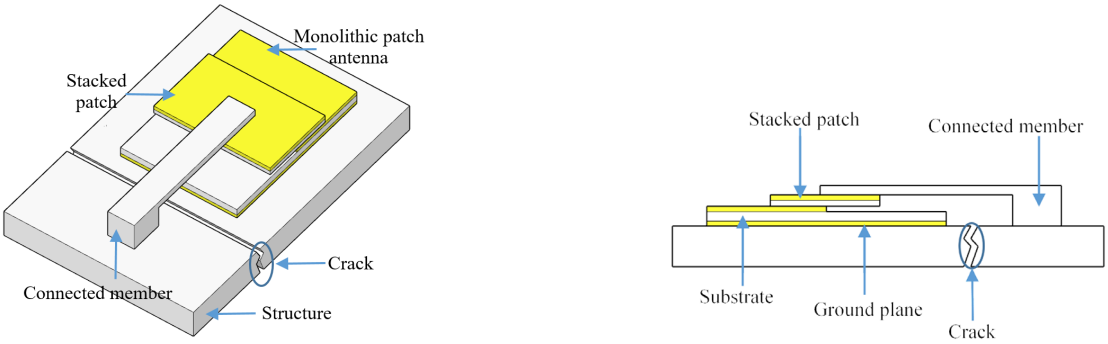

(a) Axonometric drawing (b) Front view

Fig. 2 Concept of crack sensor applied in structure using a two-layer patch antenna

antenna is defined by the size of the loop in the impedance locus, which has proved to be greatest when the stacked patch is centered directly over the radiation patch of monolithic patch antenna, and decreases significantly as the patch is offset in the direction of resonance (Waterhouse 2007). The effective length of the bottom radiation patch and stacked patch would be changed as the fringing fields on the lower patch are manipulated by the offset of the stacked patch (Chung and Mohan 2003), and the resonant frequencies are further affected by the change of effective length (Balanis 2016).

A two-layer microstrip patch antenna serves as a crack sensor in Fig. 2 for the simplest structure in a multilayer microstrip patch antenna. This two-layer patch antenna consists of a bottom monolithic patch antenna and one stacked patch. The stacked patch is formed by another parallel radiation patch and a dielectric board between these two radiation patches. The two radiation patches disconnect with each other and form an open circuit. Two resonant frequencies are determined by the length of the radiation patches and become shifted by the coupling change, which is affected by the location of the stacked patch.

For practical use, taking crack monitoring as an example, the bottom monolithic patch antenna is placed on one side of the crack, and the stacked patch is connected with another side by the connected member, which is shown in Fig. 2. Once the crack is expanded, the relative position between the patch antenna and the movable stacked patch will change and lead to a coupling change of the two-layer microstrip patch antenna, which produces the crack sensor's shift in resonant frequencies. By the way, this antenna sensor could be further used to monitor the relative displacement directly. The average stress in the structure surface could also be detected if the initial displacement between the monolithic patch antenna and stacked patch is determined.

2.1 Theory of two-layer patch antenna sensor

The resonant frequencies of a normal monolithic patch antenna can be calculated by Eq. (1) (Balanis 2016).

$$f_{mn} = \frac{c}{2\pi\sqrt{\varepsilon}}\sqrt{\left(\frac{m\pi}{L_e}\right)^2 + \left(\frac{n\pi}{W_e}\right)^2} \tag{1}$$

where L_e is the electrical length and W_e is the electrical width; m and n represent the order in the longitudinal direction and transverse direction, respectively. c is the speed of light; ε is the dielectric constant of the dielectric

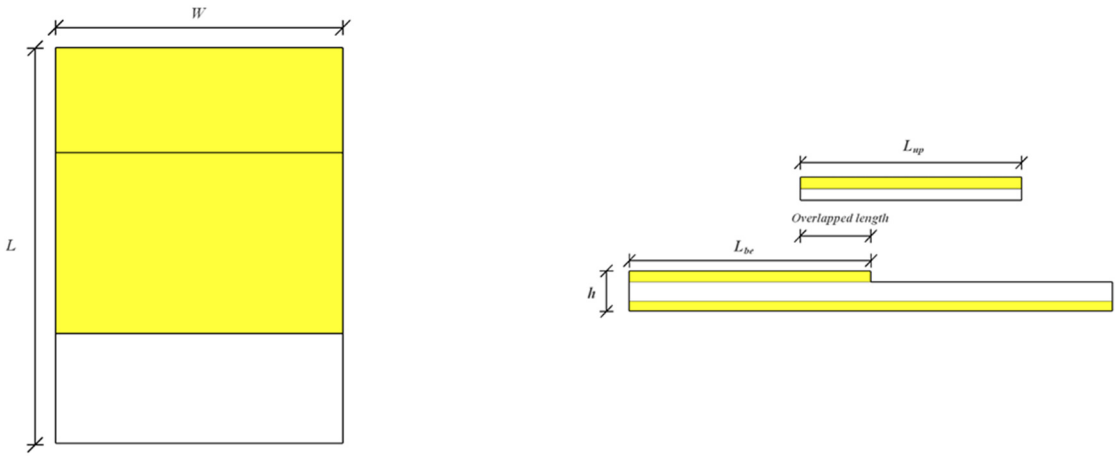

(a) Top view (b) Front view

Fig. 3 Dimensional drawing of designed two-layer patch antenna

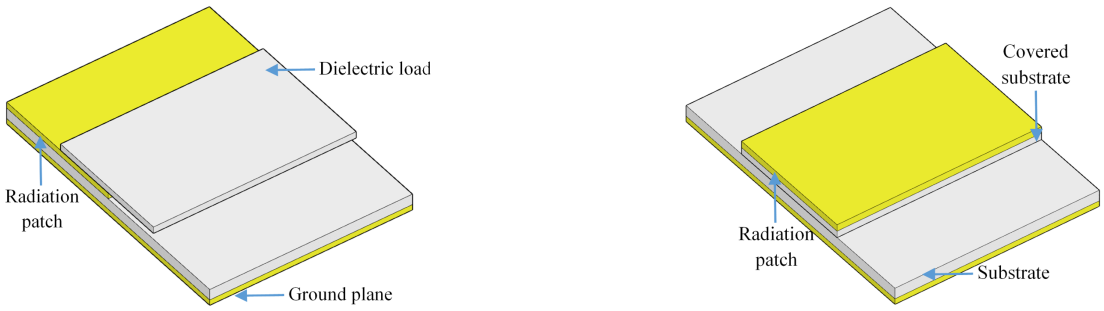

(a) Monolithic patch antenna with dielectric load (b) Monolithic patch antenna with two-layer substrate

Fig. 4 Concept of two equivalent patch antennas with different resonant radiation patch

substrate; f_{mn} is the resonant frequency when the antenna is resonant at the m order in the longitudinal direction and the n order in a transverse direction.

If we ignore the influence of coupling between the two radiation patches, the resonant frequencies of a two-layer patch antenna can be calculated by dividing the configuration into two special cases of a monolithic patch antenna and determining the resonance of each (Rajo-Iglesias *et al*. 2001). In general, a simplified two-layer patch antenna, as shown in Fig. 3, can be equivalent to a bottom monolithic patch antenna with a dielectric load and a monolithic patch antenna with a two-layer substrate, which are shown in Fig. 4.

Obviously, the two fundamental resonant frequencies of the two-layer patch antenna are the fundamental resonant frequencies of the two equivalent monolithic patch antennas. Similar to the monolithic patch antenna, the resonant frequencies of the two-layer patch antenna can be calculated by Eqs. (2) and (3), respectively (Rajo-Iglesias *et al*. 2004, Hassani and Mirshekar-Syahkal 1995)

$$f_{up-mn} = \frac{c}{2\pi\sqrt{\varepsilon_{up}}}\sqrt{\left(\frac{m\pi}{L_{up-e}}\right)^2 + \left(\frac{n\pi}{W_{up-e}}\right)^2} \tag{2}$$

where L_{up-e} is the electrical lengths of the upper antennas; W_{up-e} is the electrical width; h is the height of the monolithic patch antenna; m and n are the orders in the longitudinal direction and transverse direction, respectively. c is the speed of light; ε_{up} is the dielectric constant of the dielectric substrate; f_{up-mn} is the resonant frequency when the upper antenna is resonant at the m order in the longitudinal direction and the n order in transverse direction.

$$f_{be-mn} = \frac{c}{2\pi\sqrt{\varepsilon_{be}}}\sqrt{\left(\frac{m\pi}{L_{be-e}}\right)^2 + \left(\frac{n\pi}{W_{be-e}}\right)^2} \tag{3}$$

where L_{be-e} is the electrical lengths of the bottom antennas; W_{be-e} is the electrical width; ε_{up} is the dielectric constant of the dielectric substrate; f_{be-mn} is the resonant frequency when the bottom antenna is resonant at the m orders in the longitudinal direction and at the n orders in transverse direction.

Then the fundamental resonant frequencies in the longitude direction of these two monolithic patch antennas can be calculated respectively as

$$f_{up-10} = \frac{c}{2L_{up-e}\sqrt{\varepsilon_{up}}} \tag{4}$$

where f_{up-10} is the fundamental resonant frequency of the upper patch antenna, and

$$f_{be-10} = \frac{c}{2L_{be-e}\sqrt{\varepsilon_{be}}} \tag{5}$$

where f_{be-10} is the fundamental resonant frequency of the lower patch antenna.

The electric length can be calculated from the geometric dimensions of the radiation patch and the fringe extensions as

$$L_e = L + \Delta L \tag{6}$$

where L is the length of the radiation patch and ΔL is the line extension. As the substrate height, h, is much smaller than the dimensions of the radiation patch, the line extension ΔL can be neglected (Bernhard and Tousignant 1999). Therefore, Eqs. (4) and (5) can be reduced to

$$f_{be-10} = \frac{c}{2L_{be}\sqrt{\varepsilon_{be}}} \tag{7}$$

and

$$f_{up-10} = \frac{c}{2L_{up}\sqrt{\varepsilon_{up}}} \tag{8}$$

where L_{be} and L_{up} are the length of the radiation patch and are stacked patch, respectively.

The equivalent models in Fig. 4 can primarily calculate the range of two fundamental resonant frequencies, but the coupling effect is not considered in this method. In order to analyze the coupling fact, two equivalent models are proposed and the effect of the sub-patch movement had been quantitatively calculated, which is shown in the Section 2.2 and 2.3.

2.2 Offset of the stacked patch

The bottom monolithic patch antenna of a normal two-layer patch antenna can be modeled by an equivalent

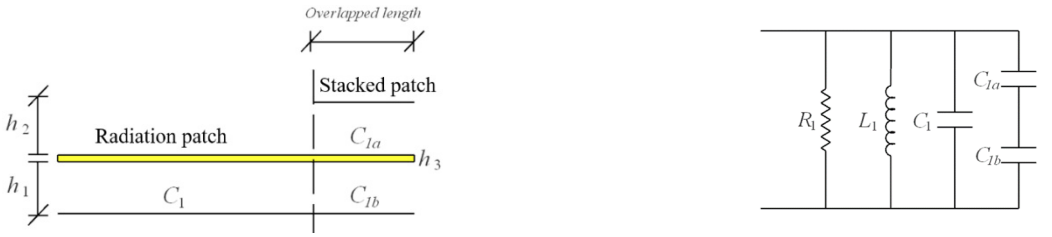

(a) Schematic map (b) Equivalent circuit

Fig. 5 Equivalent circuit of bottom monolithic patch antenna

circuit, and the influence of the stacked patch can be described by adding a series capacitance, which is shown in Fig. 5.

In Fig. 5, R_1 and L_1 are the equivalent impedance and equivalent inductance of the bottom patch antenna; C_1 is the equivalent capacitance at the uncovered region of the stacked patch; C_{1a} and C_{1b} are the series capacitance at the overlapped region; h_1 and h_2 are the thickness of monolithic patch antenna and stacked substrate, and h_3 is the thickness of the stacked copper patch.

Assuming the dielectric constant of the bottom substrate is equal to the dielectric constant of the stacked substrate, these parameters can be calculated by equation (9) in the following manner

$$L_1 = \frac{\mu h_1 L_{be}}{W} \tag{9}$$

$$C_1 = \frac{W(L_{be} - L_{ov})\varepsilon}{h_1} \tag{10}$$

$$C_{1a} = \frac{WL_{ov}\varepsilon}{h_2} \tag{11}$$

$$C_{1b} = \frac{WL_{ov}\varepsilon}{h_1} \tag{12}$$

where μ is the permeability of the substrate.

The whole equivalent capacitance of the bottom patch antenna can be calculated by Eq. (13)

$$C_{be} = C_1 + \frac{C_{1a}C_{1b}}{C_{1a} + C_{1b}} = \frac{W(L_{be} - L_{ov})\varepsilon}{h_1} + \frac{WL_{ov}\varepsilon}{h_1 + h_2} \tag{13}$$

Then, the fundamental resonant frequency of the bottom patch antenna can be calculated by Eq. (15)

$$f_{be} = \frac{1}{2\pi\sqrt{C_{be}L_1}} = \frac{c}{2\sqrt{\left(\frac{(L_{be} - L_{ov})\varepsilon}{h_1} + \frac{L_{ov}\varepsilon}{h_1 + h_2}\right)h_1 L_{be}}} \tag{14}$$

Rewritten Eq. (15)

$$\begin{aligned} f_{be} &= \frac{c}{2\sqrt{\varepsilon[L_{be} - (1-k)L_{ov}]L_{be}}} \\ &= \frac{c\sqrt{L_{be} + (1-k)L_{ov}}}{2\sqrt{\varepsilon[L_{be}^2 - (1-k)^2 L_{ov}^2]L_{be}}} \end{aligned} \tag{15}$$

where k is defined by

$$k = \frac{h_1}{h_1 + h_2} \tag{16}$$

As the overlapped length is trivial compared with the length of the radiation patch, Eq. (16) can be rewritten as

$$f_{be} \approx \frac{c\sqrt{L_{be} + (1-k)L_{ov}}}{2L_{be}\sqrt{\varepsilon L_{be}}} \tag{17}$$

That is, the fundamental resonant frequency of the bottom monolithic patch antenna would increase with the increasing of the overlapped length.

Analogously, for the stacked patch, the influence of the monolithic patch antenna can be analyzed by adding a series capacitance, which is shown in Fig. 6.

In Fig. 6, R_2 and L_2 are the equivalent impedance and equivalent inductance of the stacked patch, and C_2 is the

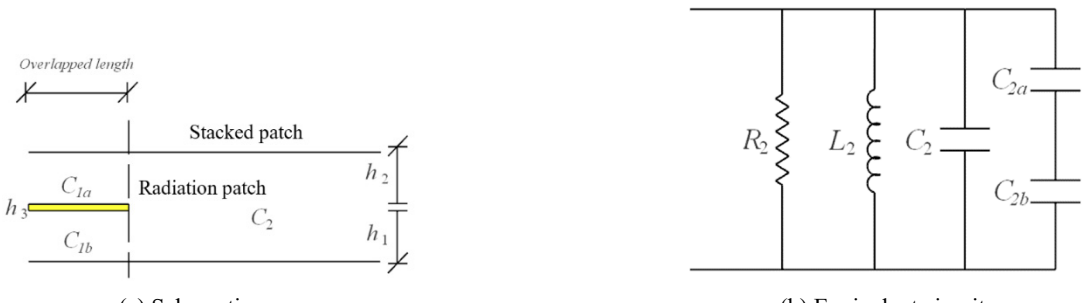

(a) Schematic map (b) Equivalent circuit

Fig. 6 Equivalent circuit of stacked patch

equivalent capacitance at the uncovered region of the stacked patch.

Similar to the bottom patch antenna, the fundamental resonant frequency of the stacked patch can be calculated by Eq. (17)

$$f_{up} = \frac{c}{2\sqrt{\varepsilon\left(L_{up} + gL_{ov}\right)L_{up}}} = \frac{c\sqrt{L_{up} - gL_{ov}}}{2\sqrt{\varepsilon(L_{up}^2 - g^2L_{ov}^2)L_{up}}} \approx \frac{c\sqrt{L_{up} - gL_{ov}}}{2\sqrt{\varepsilon L_{up}^2 L_{up}}} \quad (18)$$

where the g can be expressed as

$$g = \frac{h_3}{h_1 + h_2} \quad (19)$$

From Eq. (17), the fundamental resonant frequency of the stacked patch antenna will decrease with the increasing of overlapped length. Combining Eqs. (16) and (17), we can find that when the two antennas are away from each other, the coupling effect was weakened, and this relative movement would tend to separate the two existing resonant frequencies, which is consistent with Rajo-Iglesias's work (2001, 2004).

In general, there is a dielectric board between two radiation patches. The offset of the stacked patch will affect the dielectric load, and further influence the effective length of the of the monolithic patch antenna (Bernhard and Tousignant 1999, Li and Bowler 2010). By the way, since these two monolithic patch antennas are coupled with each other, the current would exist mainly in the overlapped region of two radiation patches, and the dislocation of the stacked patch would further shift the electrical length of these two radiation patches. Because it is difficult to calculate the exact impact of the stacked patch's offset theoretically, the influence was investigated in a simulation using Ansoft HFSS and then further verified by an experiment, which is shown in Sections 3 and 4.

2.3 Method for managing resonant frequencies

Some errors can be caused in the measurement of resonant frequencies, which is shown in Eqs. (19) and (20).

$$f_{be} = f_{be-10} + err_{be} \quad (20)$$

$$f_{up} = f_{up-10} + err_{up} \quad (21)$$

where f_{be} and f_{up} are the measured fundamental resonant frequencies, while err_{be} and err_{up} are the errors caused in measurement of the resonant frequencies, respectively.

The accuracy of measurement would be influenced by these errors obviously. To reduce the impact of these errors, the two resonant frequencies are combined in Eq. (21). As the Eq. (22) shown, the error after combining the resonant frequencies would be smaller than the maximum value of the original errors, that is, the risk of the error could be decreased by the combined method, thereby increasing the accuracy of the measurement system.

$$f_{con} = \frac{\left|f_{be} - f_{up}\right|}{2} \quad (22)$$

where f_{con} is the combined frequency. Furthermore

$$|err_{con}| = \left|\frac{err_{be} - err_{up}}{2}\right| < max\left(|err_{be}|, |err_{up}|\right) \quad (23)$$

where err_{con} is the error of the combined frequency.

2.4 Design of deformation sensor

Previous works have provided some basic rules for the design of two-layer patch antennas. According to Rajo-Iglesias's work (2001), the length of the stacked patch should be lower than the length of the bottom monolithic patch antenna to enlarge the variations of the resonant frequencies per 1 millimeter. Since the relative movement along the width direction was not expected to affect antenna frequency behavior, it would not modify the effective length of the resonant side; thus, the width of the stacked patch was designed to equal the width of the monolithic patch antenna to simplify installation. Furthermore, the difference between the two fundamental resonant frequencies was greater than 1 GHz to avoid frequency spectrum overlapping (Waterhouse 2007). To simplify the antenna design, the height of the bottom patch antenna was set to equal the stacked patch.

Deferring to these rules, the parameters of the two-layer patch antenna used in this paper were designed in the authors' preliminary study. Because the stacked patch should be parallel to the bottom monolithic patch antenna, the stacked patch was designed as a sandwich consisting of two dielectric boards and a copper sheet in the middle to stiffen the patch, which is shown in Fig. 3. The length of the stacked patch and the radiation patch of the monolithic patch antenna can be calculated by Eqs. (4) and (5), and the width of the monolithic patch antenna $W$is determined as follows (Balanis 2016)

$$W \leq \frac{c}{2f_{be}}\sqrt{\frac{\varepsilon_e + 1}{2}} \quad (24)$$

Based on Eqs. (4) to (6), the basic parameters of the antenna were calculated and listed in Table 1.

Then the preliminary parameters defined in Table 1 were further confirmed by simulation using the Ansoft High Frequency Structure Simulator (HFSS) software to ensure

Table 1 Setting domain for parameters of the deformation sensor

Parameters	W (mm)	L_{be} (mm)	L_{up} (mm)	$f_{up} - f_{be}$ (GHz)	$\boldsymbol{\varepsilon_e}$	$\boldsymbol{k}$	$\boldsymbol{h_1}$ (mm)	$\boldsymbol{h_3}$ (mm)
Dimensions	< 35	18-22	13-18	1-2	2.2	1	0.508	0.035

the working performance, which is shown in Section 3.

3. Modeling and simulation

Some radiation properties of the crack sensor are simulated using the Ansoft HFSS. Both the wired and wireless model of the two-layer patch antenna proposed in Section 2 were analyzed in Ansoft HFSS to compare the impact of the feed method. The basic parameters were confirmed at first to ensure the workability of the antenna sensor. Then, the current distributions of each resonant mode were studied to confirm the design theory proposed in Section 2. Finally, the relationship between the fundamental resonant frequencies and relative movements was investigated by simulation both in wired and wireless models. Some comparisons were also made between the wired simulation and wireless simulation.

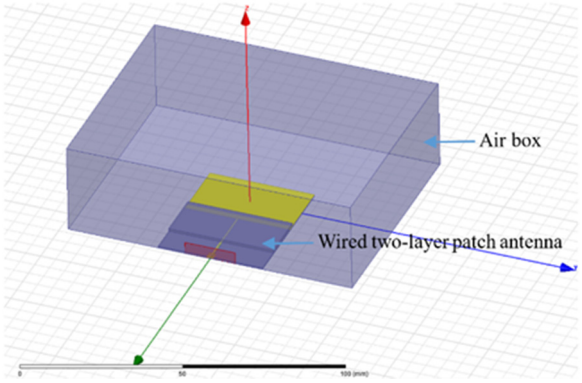

Fig. 7 Wired model of deformation sensor in HFSS

3.1 Wired simulation for a two-layer patch antenna sensor

Fig. 7 shows the wired HFSS model, which consists of a patch antenna and a stacked patch. The radiation patch is made of copper. The stacked patch is made up of a copper sheet and a coated dielectric board. Both the dielectric board material and the substrate is the Rogers RT/® Duroid 5880. An air box with a radius of about a quarter wavelength is used to contain the deformation sensor to ensure the computational accuracy of far field radiation. The bottom monolithic patch antenna is fed by a wave port connected to the microstrip line. The boundary condition of the ground plane was selected as Perfect E based on its perfect perpendicular relationship to the electric field surface.

The model was optimized by changing the basic parameters of the model within the range of Table 1, and the parameters with best antenna performance are shown in Table 2.

Given these parameters in Eqs. (16) and (17), the relationship between the overlapped length and two resonant frequencies are shown in Fig. 8. The theoretical results show an absolutely linear relationship between the overlapped length and resonant frequency shifts.

Then the current distributions at the 1st resonant frequency of underlying patch were investigated. The results are shown in Fig. 9. The current flows from the bottom microstrip line to the radiation patch and then affects the upper radiation patch by the coupling. For both radiation patches, the current mainly existed in the surface of the overlapped location, which inferred that the two-patch antenna were coupled with each other.

The simulation of the deformation sensor with the moving stacked patch is carried out after the current

Table 2 Optimized parameters of the deformation sensor

Parameters	W (mm)	L_{be} (mm)	L_{up} (mm)	f_{up} (GHz)	f_{be} (GHz)	$\boldsymbol{\varepsilon_e}$	$\boldsymbol{k}$
Dimensions	35	20.6	16	4.2	6	2.2	1

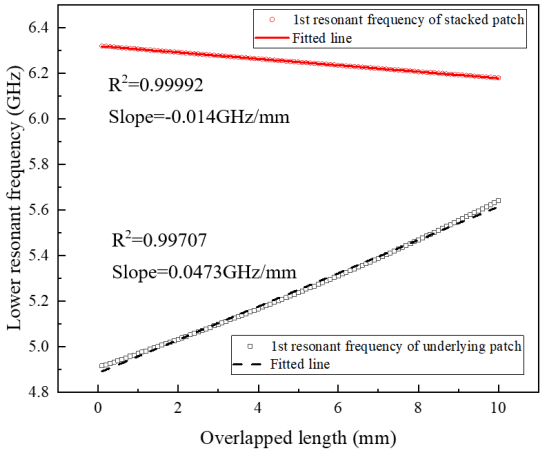

(a) 1st resonant frequency of underlying patch and stacked patch

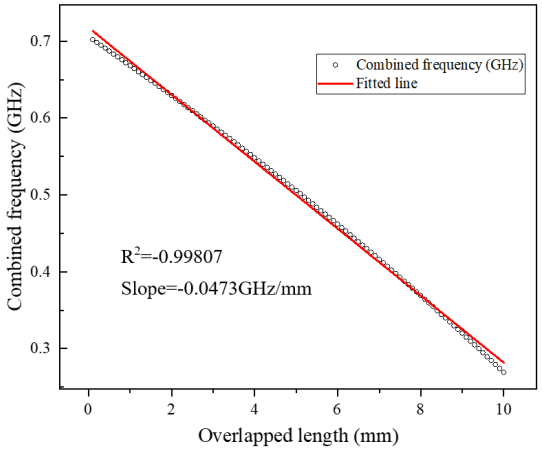

(b) Combined frequency

Fig. 8 Theoretical relationship between fundamental resonant frequencies and relative displacement

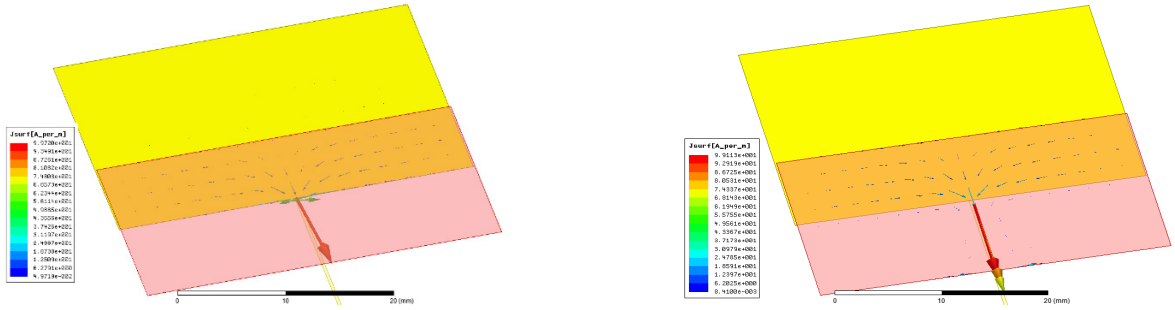

(a) Surface of radiation patch (b) Surface of the stacked patch

Fig. 9 Current distributions in wired model

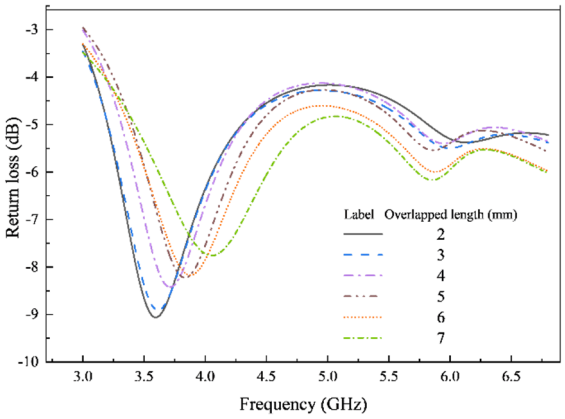

Fig. 10 The return loss curve of the simulated wired model in a wide range

distribution analysis. The initial overlapped length was set as 2 mm and then approached to 7 mm. During the whole process, the upper patch approaches the wave port and the movement becomes constrained to displacements along the axis z, thereby corresponding to the resonant side until the relative displacement achieves 6 mm.

One step of the movement is set at 0.1 mm. The return loss curves around two fundamental resonant frequencies that are acquired for each moving step, as shown in figure 10. Two fundamental resonant frequencies of the two-layer deformation sensor are then extracted from each of the return loss curves. Fig. 11 plots the relationship between fundamental resonant frequencies and overlapped length (which represents the relative displacements), using a scatter diagram.

Fig. 11(a) shows a nearly linear relationship between the relative displacement and two resonant frequencies. The sensitivity coefficient of the deformation sensor shown by the slopes of two fitted lines are 0.095 GHz/mm and 0.048 GHz/mm. After combining these two fundamental resonant frequencies by Eq. (21) the relationship between the relative displacement and the combined frequency f_{con} is shown in Fig. 8(b).

The correlation coefficients of two fitted lines in Fig. 8(a) are 0.9395 and 0.8564 respectively, which shows the resonant frequencies to nearly shift linearly with the increasing of relative displacement. After the two resonant frequencies are combined, the correlation coefficient of the fitted line in Fig. 8(b) increases to 0.9575; thus, the measured accuracy is increased by combining the two fundamental resonant frequencies.

3.2 Wireless simulation for two-layer patch antenna sensor

Fig. 12 shows the wireless HFSS model. Compared to

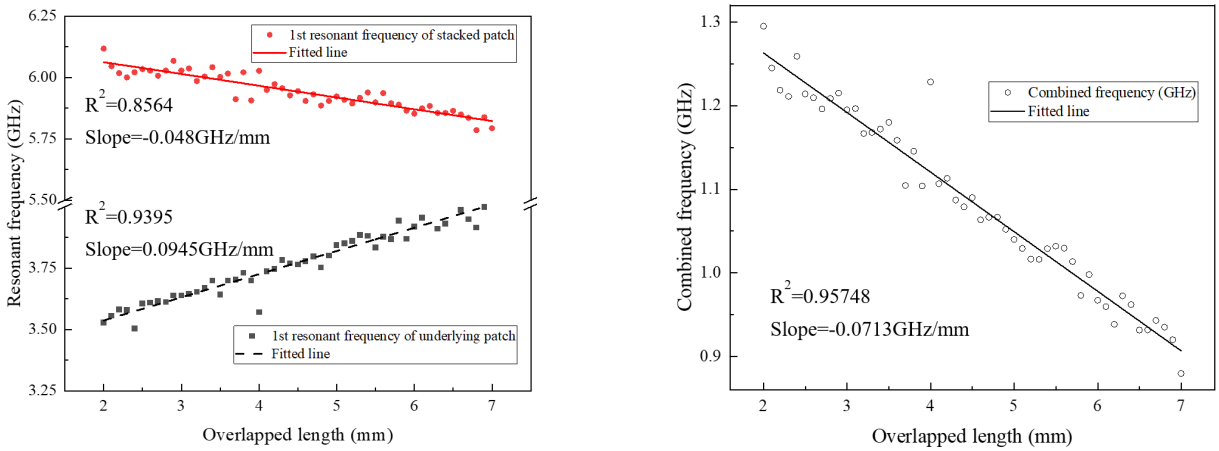

(a) 1st resonant frequency of underlying patch and stacked patch (b) Combined frequency

Fig. 11 Relationship between two fundamental resonant frequencies and relative displacement in the simulated wired model

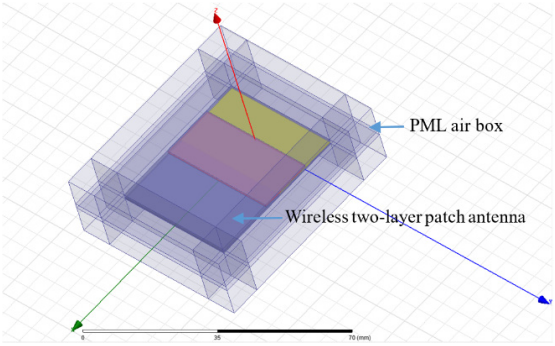

Fig. 12 Wireless model of deformation sensor in HFSS

the wired model in Section 3.1, the microstrip line is removed from the bottom monolithic patch antenna as the whole antenna is fed by the plane wave. The deformation sensor is arranged inside a perfectly matched layer (PML) air box. The whole system is fed by a plane wave above the patch antenna. Other components of the antenna sensor stay the same with the wired form.

The current distributions for the wireless types at the two fundamental resonant modes are investigated and shown in Fig. 13. Since the feeding from plane wave was uniform for two radiation patches, the TM01 resonant mode clearly appears in the current distribution figures, which suggest that the 1st resonant frequency of underlying patch is caused by the resonance of the monolithic patch antenna as shown in Fig. 13(a), and the 1st resonant frequency of stacked patch is caused by the resonance of the stacked patch as shown in Fig. 13(b).

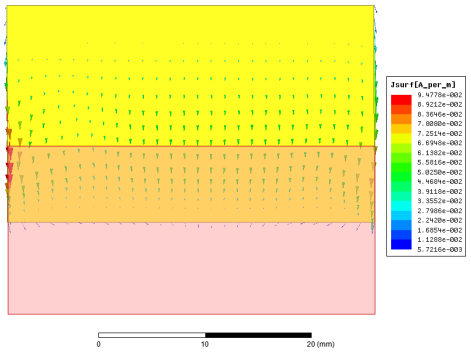

(a) Surface of radiation patch

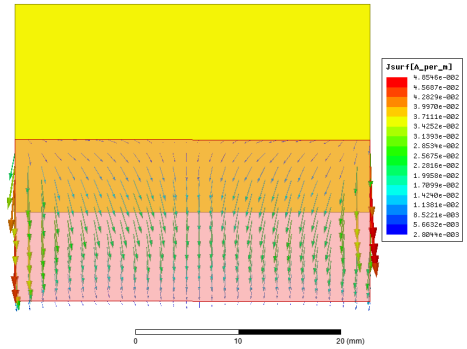

(b) Surface of the stacked patch

Fig. 13 Current distributions in wireless model

Then the simulation of the deformation sensor is carried out as offset in the stacked patch. The overlapped length ranged from 11 mm and to 14 mm, and the moving step remained the same as the wired type. To compare the

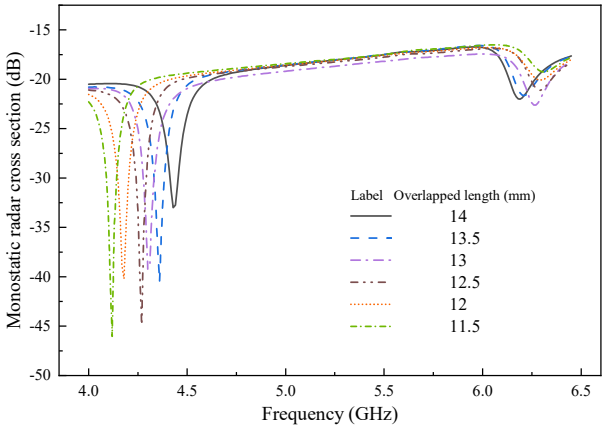

Fig. 14 Monostatic radar cross section (RCS) curve of the simulated wireless model in a wide range

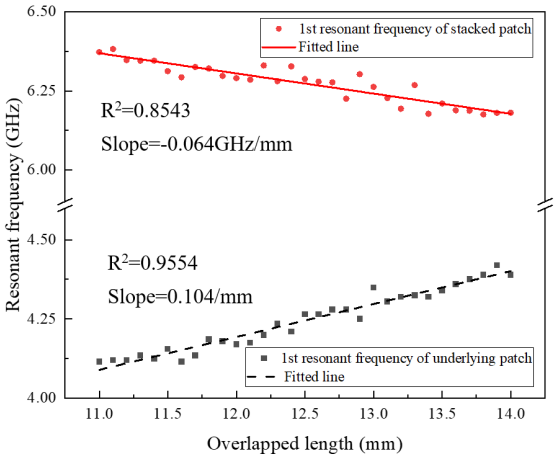

(a) 1st resonant frequency of underlying patch and stacked patch

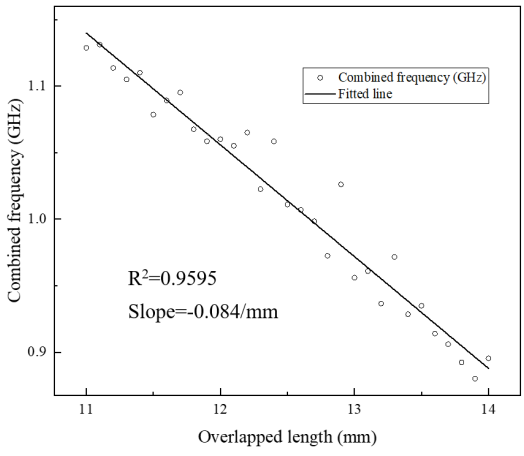

(b) Combined frequency

Fig. 15 Relationship between two fundamental resonant frequencies and relative displacement in the simulated wireless model

wireless results with the wired results, the monostatic radar cross section (RCS) curve around the two fundamental resonant frequencies is acquired for each moving step, as shown in Fig. 14. Furthermore, a scatter diagram of two fundamental resonant frequencies and relative displacements are plotted in Fig. 15.

The correlation coefficients of the two fitted lines in Fig. 15(a) are 0.9554 and 0.8543 respectively, while the correlation coefficient of the fitted line in Fig. 15(b) is 0.9595. It is obvious that the accuracy could be increased by combining the two fundamental resonant frequencies, which is same as that shown in the wired model results. Since the radiation boundary, interrogating method, and environmental situation in simulation are different than that found in the actual occurrence, some experiments were designed to verify the performance of the proposed sensor. The procedures are defined in Section 4.

4. Experiments

For testing, the materials used to fabricate sensors were copper and RT/Duroid 5880, which remain the same with the simulated models in Section 3. The workability of both the wired and wireless type sensors were measured and then compared with the simulated results. The parameters used to make the antenna sensor are the same as those listed in Table 2.

4.1 Instrumentation setup

The experiments were carried out using the testing device shown in Fig.16. A micrometer was used to form the deformation measured in the experiments. The micrometer consists of a fixed table, a fine-tuning table, and a screw type micrometer rod. The bottom monolithic patch antenna was connected to a fixed table, while the stacked patch was connected to the fine-tuning table. Because the displacement between the fixed table and the fine-tuning table could be adjusted by the screw type micrometer rod with a resolution of 0.1 mm, a width-adjustable crack was formed, which then caused a relative movement between the bottle patch antenna and the stacked patch, thereby changing the fundamental resonant frequencies of the two-layer patch antenna sensor.

For the wired type, the sensor was fed by the microstrip line at the end of the bottom monolithic patch antenna. For the wireless type, a wide-band antenna was used to give

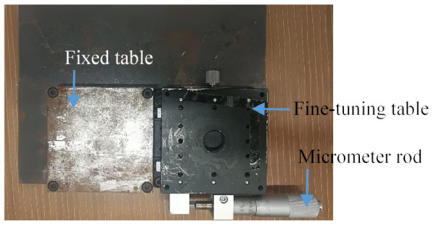

(a) Micrometer

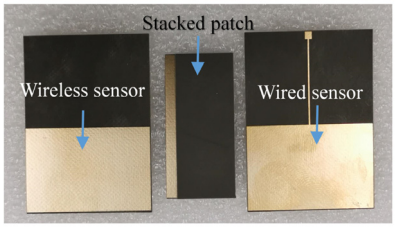

(b) Wired and wireless deformation sensor

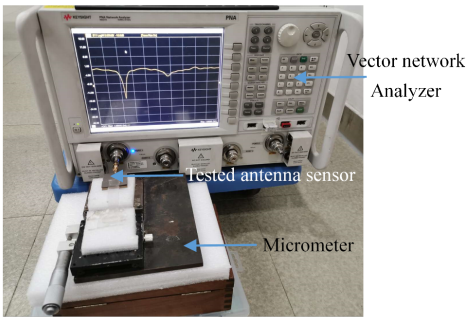

(c) Testing wired deformation sensor

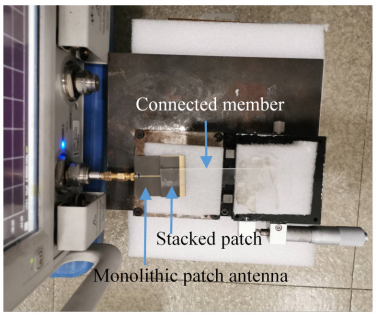

(d) Micrometer with the wired deformation sensor

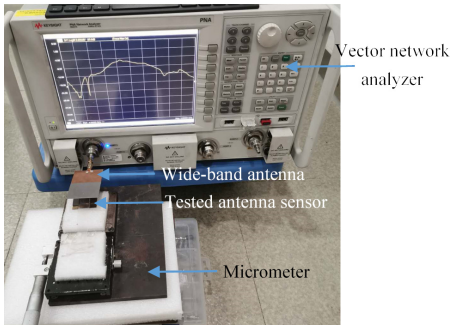

(e) Testing wireless deformation sensor

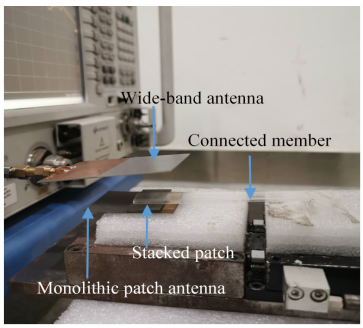

(f) Micrometer with a wireless deformation sensor

Fig. 16 The experimental setup

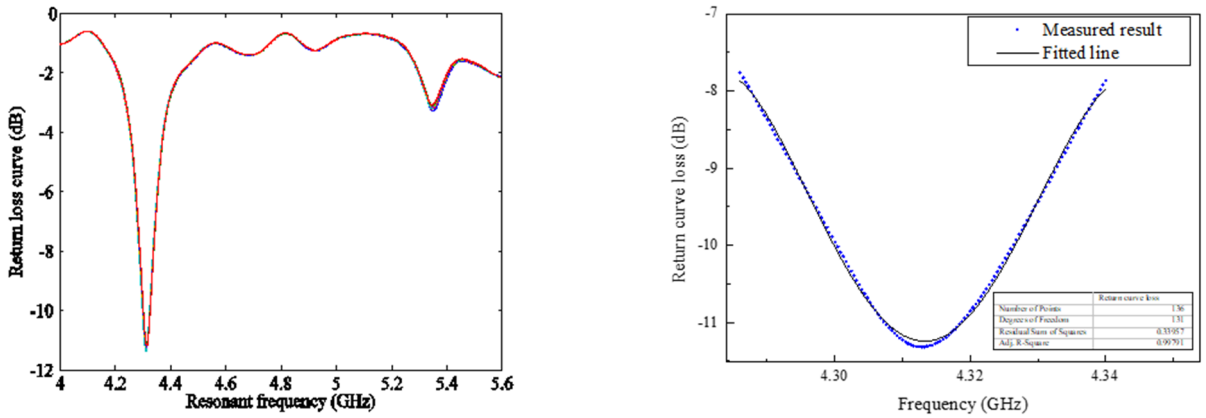

(a) Original return curve loss (b) Fitted curve

Fig. 17 Comparison of measured points and fitted curve

Table 5 Sensitivity and correlation coefficient in wired experiment

Parameters	1st resonant frequency of stacked patch	1st resonant frequency of underlying patch	Combined frequencies
Sensitivity (GHz/mm)	0.0279	0.0033	-0.0156
1st Correlation Coefficient	0.9450	0.9283	0.9469

a plane wave feeding to the sensor and, thus, to receive the backscattering of the patch antenna. The wide-band antenna shown in Fig. 16 was made in the authors' labs according to some previous research (Xue *et al.* 2019a, b, c). The displacement between the wide-band antenna and the antenna sensor was set at about 3 cm to ensure the strength of the backscattering and further reduce the background reflection. A vector network analyzer (VNA) was used to analyze the signal received from the wired deformation sensor or the wide-band antenna. The wired and wireless experiments were carried out with the relative displacement changing and yet the results kept remained the same as the works in simulation and the experimental results are shown in Section 4.2.

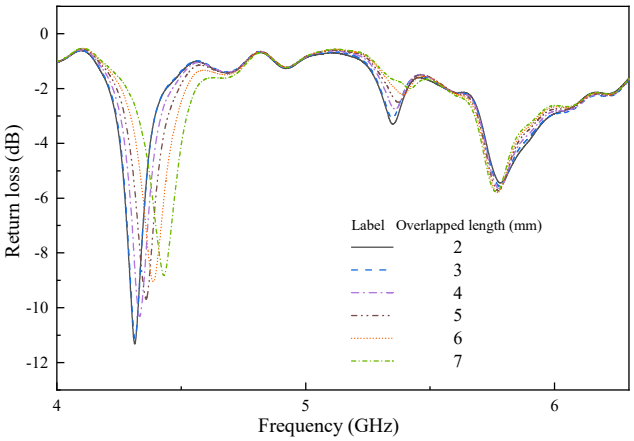

Fig. 18 Return loss curve in wired experiment

4.2 Results and discussion

The return loss curves and RCS curves obtained from the experiments are analyzed in this Section. To reduce the experimental error, these curves of the deformation sensor are tested three times and averaged at each incremental step. The cubic polynomial curve is utilized to fit these curves around the area of desired resonant frequencies, and the resonant frequency at the local minimum is extracted for each curve. The comparison of measured points and the fitted curve around the desired resonant frequencies is shown in Fig. 17. Furthermore, some discussion about the wired and wireless type antenna sensor is shown in Sections 4.2.1 and 4.2.2.

4.2.1 Wired experiment results for two-layer patch antenna sensor

The return-loss curve in the wired experiment is shown in Fig. 18. Furthermore, the sensitivity and correlation coefficient extracted from the fitted lines are shown in Table 5.

The scatter diagram of the resonant frequency and relative displacement for each resonant frequency are then plotted in Fig. 19(a), which is compared with the combined results shown in Fig. 19(b).

The 1st correlation coefficients for the upper and bottom resonant frequency are 0.9283 and 0.9450, while the 1st correlation coefficients of the combined resonant frequency are 0.9506. It is obvious that the workability increased, because the 1st correlation coefficient of the combined resonant frequency is close to the 1st correlation coefficient of the resonant frequency with a better performance. Furthermore, the 1st correlation coefficient increases after the two resonant frequencies are combined, which means the accuracy could be increased in this way.

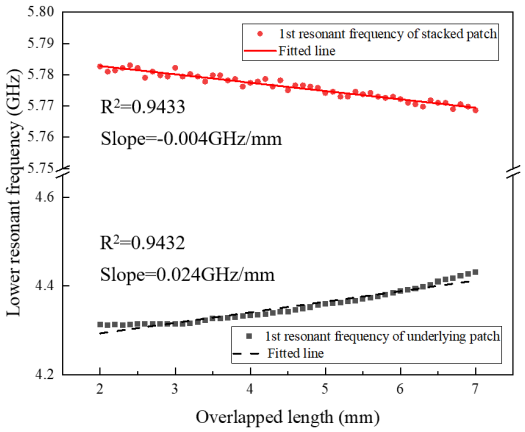

(a) 1st resonant frequency of underlying patch and stacked patch

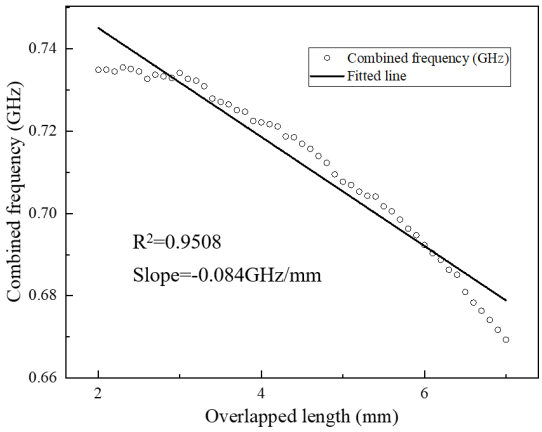

(b) Combined frequency

Fig. 19 Relationship between two fundamental resonant frequencies and relative displacement in the wired experiment

Table 6 Sensitivity and correlation coefficient in wireless experiment

Parameters	1st resonant frequency of stacked patch	1st resonant frequency of underlying patch	Combined frequency
Sensitivity (GHz/mm)	−0.068	0.055	−0.061
1st Correlation Coefficient	0.9929	0.9913	0.9943

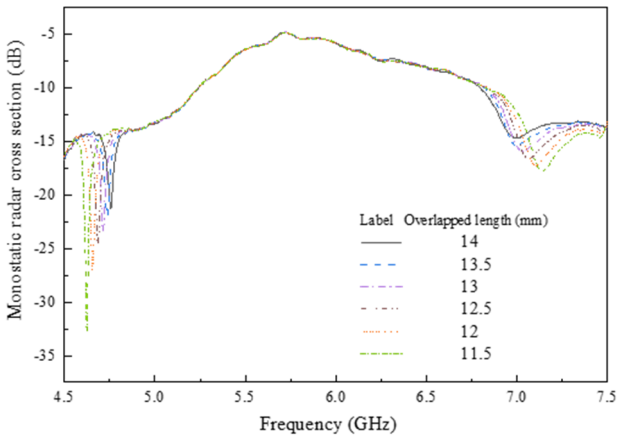

Fig. 20 Radar cross section curve in wireless experiment

4.2.2 Wireless experiment results for two-layer patch antenna sensor

The monolithic radar cross section curve in wireless experiment is shown in Fig. 20, while the sensitivity and correlation coefficient extracted from the fitted lines are shown in Table 6. Analogous to the wired experiment, two scatter diagrams are used to analyze the relationship between the resonant frequencies and relative displacement, which are shown in Fig. 21.

Similar to the wired experiment, as shown in Fig. 21, the accuracy was increased after combining two fundamental resonant frequencies.

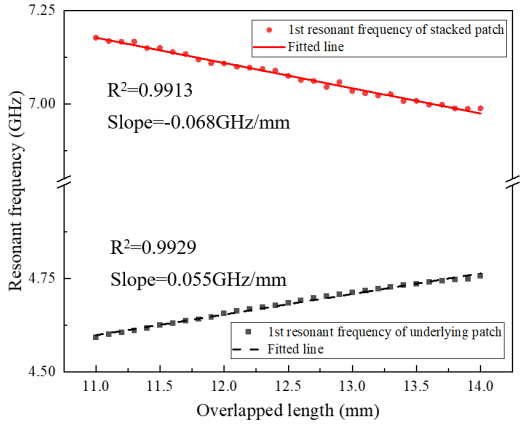

(a) 1st resonant frequency of underlying patch and stacked patch

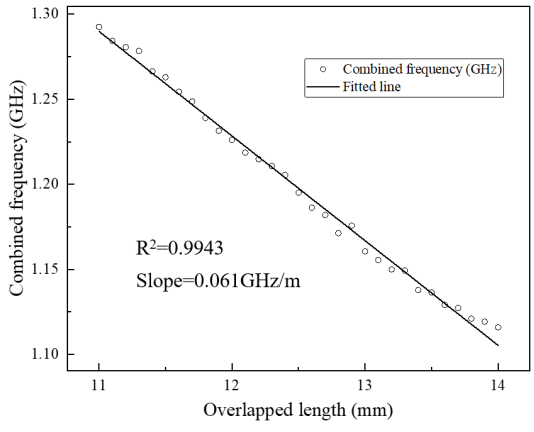

(b) Combined frequency

Fig. 21 Relationship between two fundamental resonant frequencies and relative displacement in the wireless experiment

5. Conclusions

This paper introduces an unstressed sensor based on a two-layer patch antenna for measuring structural deformation, such as crack and displacement. We have shown that the fundamental resonant frequencies of the proposed two-layer patch antenna sensor would shift nearly linearly with the dislocation of the stacked patch due to the coupling change between the monolithic patch antenna and the stacked patch. Without the presence of stress in the antenna sensor, the crack width or displacement can be characterized by the sensor with a resolution of 0.1 mm, which is ensured by theoretical calculation, numerical simulation and experiments. In another case study, the measuring accuracy has been increased by combining two fundamental resonant frequencies. Both wired and wireless prototypes have been analyzed in each case and showed a minimum correlation coefficient of 0.95 after combining two fundamental resonant frequencies.

Acknowledgments

This research was funded by the National Natural Science Foundation of China (Grant No. 52078375), the Key Laboratory of Performance Evolution and Control for Engineering Structures (Tongji University), the Ministry of Education of the People's Republic of China (grant number 2018KF-4), and the Fundamental Research Funds for the Central Universities.

References

Abdulkarem, M., Samsudin, K., Rokhani, F.Z. and A Rasid, M.F. (2019), "Wireless sensor network for structural health monitoring: A contemporary review of technologies, challenges, and future direction", *Struct. Health Monit.*, **19**(3). https://doi.org/10.1177/1475921719854528

Alam, T., Faruque, M.R.I. and Islam, M.T. (2015), "Printed circular patch wideband antenna for wireless communication", *Informacije MIDEM*, **44**(3), 212-217.

Ayyildiz, C., Erdem, H.E., Dirikgil, T., Dugenci, O., Kocak, T., Altun, F. and Gungor, V.C. (2019), "Structure health monitoring using wireless sensor networks on structural elements", *Ad Hoc Netw.*, **82**, 68-76. https://doi.org/10.1016/j.adhoc.2018.06.011

Balanis, C.A. (2016), *Antenna Theory: Analysis and Design*, John Wiley & Sons.

Bernhard, J.T. and Tousignant, C.J. (1999), "Resonant frequencies of rectangular microstrip antennas with flush and spaced dielectric superstrates", *IEEE Trans. Antennas Propag.*, **47**(2), 302-308. https://doi.org/10.1109/8.761070

Bhattacharyya, R., Floerkemeier, C. and Sarma, S. (2009), "Towards tag antenna based sensing-An RFID displacement sensor", *Proceedings of the IEEE International Conference on RFID*, Orlando, FL, USA, April.

Cho, C., Yi, X., Li, D., Wang, Y. and Tentzeris, M.M. (2016), "Passive wireless frequency doubling antenna sensor for strain and crack sensing", *IEEE Sens. J.*, **16**(14), 5725-5733. https://doi.org/10.1109/JSEN.2016.2567221

Chung, K.L. and Mohan, A.S. (2003), "The effect of offset patch on the broadband characteristics of an electromagnetically coupled patch antenna", *Microw. Opt. Technol. Lett.*, **38**(5), 345-348. https://doi.org/10.1002/mop.11056

Da Xu, K., Zhu, J., Liao, S. and Xue, Q. (2018), "Wideband patch antenna using multiple parasitic patches and its array application with mutual coupling reduction", *IEEE Access*, **6**, 42497-42506. https://doi.org/10.1109/ACCESS.2018.2860594

Godara, L.C. (2018), "Microstrip Patch Antennas", In: *Handbook of Antennas in Wireless Communications* (pp. 190-216), CRC Press.

Hassani, H.R. and Mirshekar-Syahkal, D. (1995), "Study of electromagnetically coupled stacked rectangular patch antennas", *IEE Pro: Microw. Anten. Propag.*, **142**(1), 7-13. https://doi.org/10.1049/ip-map:19951540

Hu, J., Hao, Z.-C. and Hong, W. (2017), "Design of a wideband quad-polarization reconfigurable patch antenna array using a stacked structure", *IEEE Trans. Antennas Propag.*, **65**(6), 3014-3023. https://doi.org/10.1109/TAP.2017.2695529

Leung, C.K.Y., Elvin, N., Olson, N., Morse, T.F. and He, Y.-F. (2000), "A novel distributed optical crack sensor for concrete structures", *Eng. Fract. Mech.*, **65**(2-3), 133-148. https://doi.org/10.1016/S0013-7944(99)00112-5

Li, Y. and Bowler, N. (2010), "Resonant frequency of a rectangular patch sensor covered with multilayered dielectric structures", *IEEE Trans. Antennas Propag.*, **58**(6), 1883-1889. https://doi.org/10.1109/TAP.2010.2046871

Malekpoor, H. and Hamidkhani, M. (2019), "Compact multi-band stacked circular patch antenna for wideband applications with enhanced gain", *Electromagnetics*, **39**(4), 241-253. https://doi.org/10.1080/02726343.2019.1595379

Marindra, A.M.J. and Tian, G.Y. (2019), "Multiresonance chipless RFID sensor tag for metal defect characterization using principal component analysis", *IEEE Sens. J.*, **19**(18), 8037-8046. https://doi.org/10.1109/JSEN.2019.2917840

McGee, K., Anandarajah, P. and Collins, D. (2019), "A review of chipless remote sensing solutions based on RFID technology", *Sensors*, **19**(22), 4829. https://doi.org/10.3390/s19224829

Mohammad, I. and Huang, H. (2010), "Monitoring fatigue crack growth and opening using antenna sensors", *Smart Mater. Struct.*, **19**(5), 55023. https://doi.org/10.1088/0964-1726/19/5/055023

Mohammad, I. and Huang, H. (2012), "Pressure and shear sensing based on microstrip antennas", *Proceedings of Sensors and Smart Structures Technologies for Civil, Mechanical, and Aerospace Systems 2012*, San Diego, CA, USA, May. https://doi.org/10.1117/12.914979

Mohammad, I., Gowda, V., Zhai, H. and Huang, H. (2011), "Detecting crack orientation using patch antenna sensors", *Meas. Sci. Technol.*, **23**(1), 15102. https://doi.org/10.1088/0957-0233/23/1/015102

Moreno-Gomez, A., Perez-Ramirez, C.A., Dominguez-Gonzalez, A., Valtierra-Rodriguez, M., Chavez-Alegria, O. and Amezquita-Sanchez, J.P. (2018), "Sensors used in structural health monitoring", *Arch. Comput. Method Eng.*, **25**(4), 901-918. https://doi.org/10.1007/s11831-017-9217-4

Pandey, V.K. and Vishvakarma, B.R. (2005), "Theoretical analysis of linear array antenna of stacked patches", *In. J. Rad. Spac. Phys.*, **34**(2), 125-130.

Rajo-Iglesias, E., Segovia-Vargas, D., Vázquez-Roy, J.L., González-Posadas, V. and Martín-Pascual, C. (2001), "Bandwidth enhancement in noncentered stacked patches", *Microw. Opt. Technol. Lett.*, **31**(1), 53-56. https://doi.org/10.1002/mop.1355

Rajo-Iglesias, E., Villaseca-Sánchez, G. and Martín-Pascual, C. (2002), "Input impedance behavior in offset stacked patches", *IEEE Antennas Wirel. Propag. Lett.*, **1**, 28-30. https://doi.org/10.1109/LAWP.2002.802582

Rajo-Iglesias, E., Vázquez-Roy, J.L., Inclán-Sánchez, L., Segovia-Vargas, D., González-Posadas, V. and Martín-Pascual, C.

(2004), "Offset stacked patches behavior in an array", *Microw. Opt. Technol. Lett.*, **40**(3), 262-265. https://doi.org/10.1002/mop.11347

Sanders, J.W., Yao, J. and Huang, H. (2015), "Microstrip patch antenna temperature sensor", *IEEE Sens. J.*, **15**(9), 5312-5319. https://doi.org/10.1109/JSEN.2015.2437884

Soman, R.N., Onoufriou, T., Kyriakides, M.A., Votsis, R.A. and Chrysostomou, C.Z. (2014), "Multi-type, multi-sensor placement optimization for structural health monitoring of long span bridges", *Smart Struct. Syst., Int. J.*, **14**(1), 55-70. https://doi.org/10.12989/sss.2014.14.1.055

Tchafa, F.M. and Huang, H. (2018), "Microstrip patch antenna for simultaneous strain and temperature sensing", *Smart Mater. Struct.*, **27**(6), 65019. https://doi.org/10.1088/1361-665X/aabd47

Waterhouse, R. (2007), *Printed Antennas for Wireless Communications*, John Wiley & Sons.

Woo, S., Lee, S. and Chung, L. (2011), "Seismic response control of elastic and inelastic structures by using passive and semi-active tuned mass dampers", *Smart Struct. Syst., Int. J.*, **8**(3), 239-252. https://doi.org/10.12989/sss.2011.8.3.239

Xue, S., Yi, Z., Xie, L., Wan, G. and Ding, T. (2019a), "A passive wireless crack sensor based on patch antenna with overlapping sub-patch", *Sensors*, **19**(19), 4327. https://doi.org/10.3390/s19194327

Xue, S., Xu, K., Xie, L. and Wan, G. (2019b), "Crack sensor based on patch antenna fed by capacitive microstrip lines", *Smart Mater. Struct.*, **28**(8), 085012. https://doi.org/10.1088/1361-665X/ab2834

Xue, S., Yi, Z., Xie, L., Wan, G. and Ding, T. (2019c), "A displacement sensor based on a normal mode helical antenna", *Sensors*, **19**(17), 1-18. https://doi.org/10.3390/s19173767

Xue, S., Zheng, Z., Guan, S., Xie, L., Wan, G. and Wan, C. (2020a), "A Capacitively-Fed Inverted-F Antenna for Displacement Detection in Structural Health Monitoring", *Sensors*, **20**(18), 1-17. https://doi.org/10.3390/s20185310

Xue, S., Jiang, K., Guan, S., Xie, L., Wan, G. and Wan, C. (2020b), "Long-Range Displacement Meters Based on Chipped Circular Patch Antenna", *Sensors*, **20**(17), 1-16. https://doi.org/10.3390/s20174884

Yadava, R.L. and Vishvakarma, B.R. (2000), "Analysis of electromagnetically coupled two-layer elliptical microstrip stacked antennas", *Int. J. Electron.*, **87**(8), 981-993. https://doi.org/10.1080/002072100404631

Yao, J., Tchafa, F.M., Jain, A., Tjuatja, S. and Huang, H. (2016), "Far-field interrogation of microstrip patch antenna for temperature sensing without electronics", *IEEE Sens. J.*, **16**(19), 7053-7060. https://doi.org/10.1109/JSEN.2016.2597739

Yi, X., Cho, C., Cooper, J., Wang, Y., Tentzeris, M.M. and Leon, R.T. (2013), "Passive wireless antenna sensor for strain and crack sensing—Electromagnetic modeling, simulation, and testing", *Smart Mater. Struct.*, **22**(8), 85009. https://doi.org/10.1088/0964-1726/22/8/085009

Yi, X., Cho, C., Wang, Y. and Tentzeris, M.M. (2016), "Battery-free slotted patch antenna sensor for wireless strain and crack monitoring", *Smart Struct. Syst., Int. J.*, **18**(6), 1217-1231. https://doi.org/10.12989/sss.2016.18.6.1217

You, C., Tentzeris, M.M. and Hwang, W. (2007), "Multilayer effects on microstrip antennas for their integration with mechanical structures", *IEEE Trans. Antennas Propag.*, **55**(4), 1051-1058. https://doi.org/10.1109/TAP.2007.893401